Quaternary Science Reviews 203 (2019) 90–101

Contents lists available at ScienceDirect

Quaternary Science Reviews

journal homepage: www.elsevier.com/locate/quascirev

New approach to assessing age uncertainties – The 2300-year varve chronology from Eklutna Lake, Alaska (USA)

David Fortin [a], Nore Praet [b], Nicholas P. McKay [a], Darrell S. Kaufman [a, *], Britta J.L. Jensen [c], Peter J. Haeussler [d], Casey Buchanan [c], Marc De Batist [b]

[a] School of Earth & Sustainability, Northern Arizona University, Flagstaff, Arizona, USA
[b] Renard Centre of Marine Geology, Ghent University, Krijgslaan 281, S8 WE13, 9000, Ghent, Belgium
[c] Department of Earth and Atmospheric Sciences, University of Alberta, Edmonton, Canada
[d] U.S. Geological Survey, 4210 University Drive, Anchorage, Alaska, USA

ARTICLE INFO

Article history:
Received 5 June 2018
Received in revised form
11 October 2018
Accepted 12 October 2018
Available online 19 November 2018

Keywords:
Varve
Geochronology
Age model
Tephra
Alaska

ABSTRACT

Developing robust chronological frameworks of lacustrine sediment is central to reconstructing past environmental changes. We present varve chronologies from five sites extending back 2300 years from Eklutna Lake, in the Chugach Mountains of south-central Alaska. The chronologies are built from image analysis of high-resolution photographs and CT scans of sediment cores. The age uncertainty of each record is tested by three methods. We first present varve chronologies from individual sites and reconcile the difference in varve delimitation from two observers. The varve chronologies from each site are then compared to each other using a series of marker beds that can be traced across the lake basin. Finally, using a new Bayesian probabilistic model, we develop age models that incorporate information regarding age uncertainty from the multiple-observer method and the age distribution of marker layers from multiple cores. To evaluate the accuracy of the Bayesian model output, we used seven radiocarbon ages from terrestrial macrofossils and four tephra layers traceable across the core sites. The major-element geochemistry of the tephra layers and their ages are presented here for the first time. The Bayesian age model offers a new approach to quantifying age uncertainty in inter-correlated cores of varved sediment.

1. Introduction

Varves, or annually laminated sediments, are valuable sources of paleo climate and environmental information. Substantial efforts have recently been made to improve the reliability of varve chronologies (e.g., Staff et al., 2013; Marshall et al., 2012; Tian et al., 2005). These efforts emphasize chronologies that include estimates of the age uncertainty as well as multidisciplinary approaches to corroborate varve counts with independent dating methods (Zolitschka et al., 2015; Ojala et al., 2012). Such approaches include counts performed by independent observers, semi-automated counting methods, cross-correlation among cores, the use of radioisotopes and correlation with historically documented events. These procedures result in both qualitative and quantitative assessment of chronological uncertainty, although no single approach has emerged as the standard for deriving age uncertainty in varve chronologies.

In this study, we present varve chronologies from five core sites within Eklutna Lake, south-central Alaska, extending back 2300 years. A new Bayesian model is used to quantify the age uncertainty. The model integrates uncertainties based on a comparison of varve counts made by independent observers and a comparison of varve counts between marker beds that are cross-correlated among the core sites. Our Bayesian model incorporates these assessments as estimates of a posterior distribution of ages as a function of depth, which we compare to radiocarbon ages in a validation step. Geochemically correlated tephras found in multiple cores are used as isochrones to check the age models and the accuracy of their uncertainty estimates.

By using five cross-correlated cores, our study is based on replication of independent chronologies within the same lake, which is rarely reported in the literature. Few varved sequences

* Corresponding author.
E-mail addresses: david.fortin@nau.edu (D. Fortin), darrell.kaufman@nau.edu (D.S. Kaufman).

https://doi.org/10.1016/j.quascirev.2018.10.018
0277-3791/

have been published from Alaska, and this study constitutes the longest varve record yet reported from the state. The chronology developed here serves as a framework for multiple ongoing studies of the sedimentary sequence contained in Eklunta Lake. These include: (1) dating and enumerating seismic- and flood-generated turbidites to infer the history of earthquakes and floods, (2) quantifying the long-term changes in sediment fluxes related to glacial activity within the watershed and hydroclimate regionally, and (3) reconstructing the frequency and origin of tephra fall.

2. Study site

Eklutna Lake is located 45 km northeast of Anchorage, at 264 m asl in the Chugach State Park (Fig. 1). The elongated lake averages around 1.4 km wide and 10.5 km long (14.1 km^2). It occupies the Ekluna River valley, a glacially steepened trough, naturally dammed at its northwest end by a recessional moraine from the Pleistocene Eklutna Glacier (Brabets, 1993; Hollinger, 2002; Karlstrom, 1964). The lake has two main basins reaching depths of approximately 60 and 50 m, separated by a submerged end moraine at 30 m depth (Praet et al., 2017). In 1929, the outflow of Eklutna Lake was first modified by raising the natural threshold several meters as the lake was converted into a hydroelectric reservoir. In 1964, the Prince William Sound earthquake caused severe damage to the dam, and a new dam was built raising the level of the reservoir by approximately 5 m. The Municipality of Anchorage draws water from the lake for both hydroelectric production and human water consumption, substantially modifying the amplitude and timing of annual lake-level fluctuations.

The drainage basin of Eklutna Lake (311 km^2) is dominated by two sub-watersheds, the East Fork and the West Fork. Several smaller streams, in which the suspended sediment load is negligible, account for the remainder of the total runoff to Eklutna Lake. The watersheds of East Fork and West Fork are located within the Chugach Mountains, which comprise structurally complex and variably metamorphosed sedimentary and igneous rocks (Wilson and Hults, 2013; Mankhemthong et al., 2013). Alluvial deposits, consisting primarily of gravel and sand, are present around the lake (Brabets, 1993; Praet et al., 2017). Colluvial deposits mantle the steep slopes in East Fork and West Fork basins. Rock glaciers and their deposits are found in high-level cirques while glacial and glacio-alluvial deposits are found downstream of glaciers feeding East and West Forks.

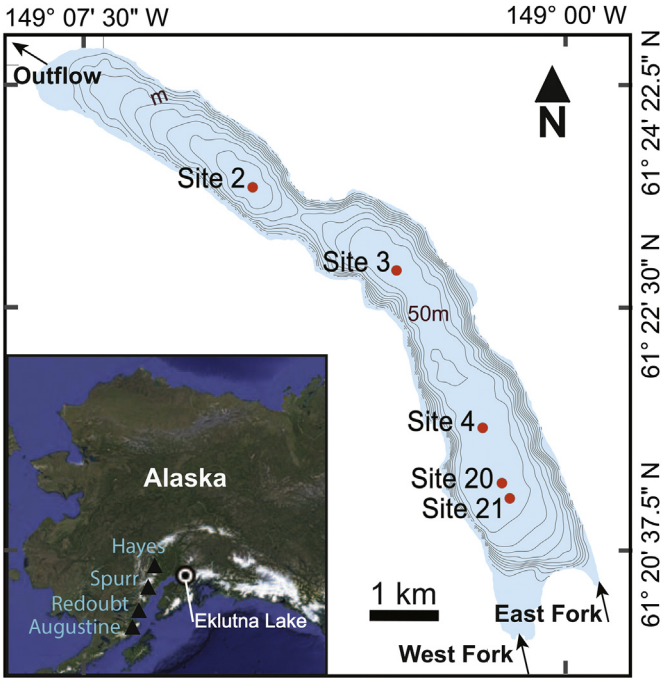

Fig. 1. Regional setting and bathymetry of Eklutna Lake with five core sites discussed. Bathymetric contour interval = 5 m. Landsat image from Google Earth.

In 2015, glaciers covered 13% of Eklutna Lake watershed (Sass et al., 2017). Numerous glaciers of various sizes include a series of small, steep glaciers in the East Fork basin (19% glacier cover) and the 12-km-long Eklutna Glacier, which covers about 48% of the West Fork watershed, making it the lake's primary water source (Hollinger, 2002). Field observations between 1975 CE and 2015 have shown that the Eklutna Glacier receded about 1.6 km over a time span of 30 years (Brabets, 1993; Sass et al., 2017).

Hydrographs for both East and West Fork are available for 1986 (Brabets, 1993) and for 2009–2010 (Larquier, 2010), and river gaging is ongoing (M. Loso and J. Osterman, unpublished). Although they exhibit significant year-to-year variations in the timing and total amount of water delivered to the lake, all monitored years show a similar seasonal trend. This pattern is characterized by an early onset of discharge in May, with a spring freshet culminating in June or early July, a peak discharge occurring in late July or early August during rain events and maximal glacier melt. The falling limb is often interrupted by significant late-summer precipitation events, until October freeze up. Median peak discharge for the period 2009–2015 is approximately 20 and 30 m^3/s for the East and the West Fork, respectively. Sediment concentration is typically higher at the West Fork than the East Fork and exhibits a strong relation with discharge. The annual pattern of discharge for these primary inflows to Eklutna Lake are similar to those described at Bench Glacier outflow by Riihimaki et al. (2005) and Allison Glacier River (Fortin et al., 2015), both in south-central Alaska. Discontinuous measurement of suspended sediment, discharge and turbidity data on both the West and East Fork for 2010 show that late summer and early fall sediment pulses during rain events represent the largest share of total sediment transfer relative to the intensity of discharge events (Larquier, 2010).

In 2012, a network of seismic profiles and surface sediment cores (~1 m long) were acquired at Eklutna Lake (Boes et al., 2018; Praet et al., 2017). These surface cores were analyzed to determine whether the prominent rhythmic layers were deposited annually (i.e., true varves) and to compare with sediment cores from two other deep glacier-fed lakes in the area (Boes et al., 2018). By cross-correlating the cores using layer counts, supported by a fine-scale sedimentary structure description, and ^{137}Cs and ^{210}Pb profiles, the study concluded that the layers found in Eklutna Lake sediments were indeed deposited annually. Historical time markers are visible in the cores, such as the 1929 failure of the reservoir dam built above the end moraine, the mass-wasting-generated turbidite resulting from the Prince William Sound earthquake of 1964 and flood-induced turbidites from 1989 to 1995. The widespread record of these events across the lake demonstrates the potential of Eklutna Lake sediments for recording historical natural and human-induced changes in the watershed. Boes et al. (2018) also showed that, after 1929, the varve couplets become less well defined in most of Eklutna Lake compared to the pre-1929 period; the upper section of the sedimentary sequence has less-distinct and thinner clay caps and darker varves, a result of the modification of lake hydrology with the construction of the dam in 1929.

3. Methods

3.1. Coring and core analysis

For this study, long sediment cores (~15 m long) were obtained in 2014 at six locations across Eklutna Lake using a Uwitec piston coring system. The cores were collected in winter from the ice surface at water depths ranging from 48 to 54.5 m (Table 1). The cores were obtained in 3-m-long sections from two overlapping contiguous holes. Total depth of the cored sequence ranged from 9 to 16 m. The 3 m sections were cut into approximately 1.5 m lengths in the field. In addition, at each coring location, a core with an undisturbed water-sediment interface was acquired using a hammer-driven gravity corer.

All core sections were shipped to Ghent University for analysis and were imaged with a medical X-ray CT scanner (Siemens SOMATOM Definition Flash). Density variations obtained from CT scans are similar to those obtained from traditional X-ray images, where dense layers of coarse sediments absorb more X-ray energy than clay particles, but without the limitations related to dispersion of X-rays and uneven thicknesses of the layers across core tubes. Volume reconstruction resulted in across-core DICOM (Digital Imaging and Communications in Medicine) images composed of 512×512 pixels (~0.16 mm/pixel) with a downcore resolution of 0.6 mm. The volume was analyzed and visualized using Volume Graphics's VGStudio 2.2 software, from which the along-core TIFF images were exported and used for varve counting. Line-scan photographs with a resolution of 300 dpi were acquired on each half-core after a careful cleaning of the core surface. Finally, the open face of every core section was scanned with a Geotek Multi-Sensor Core Logger (MSCL) at Ghent University. The acquired data include gamma-ray density, magnetic susceptibility and spectrophotometric parameters measured over steps of 0.2 cm along the central axis of the split cores.

A composite sedimentary sequence for each site was assembled from the overlapping core segments by cross-correlating marker beds visually and by choosing the least disturbed part to construct a master core (Supplementary Table S1). The overlapping core sections minimized the possibility of missing varves. Five sites were selected to undergo a more detailed analysis (Fig. 1).

3.2. Thickness measurement and varve chronologies

Using Adobe Illustrator software, varve boundaries were delimited on the center of CT-scan images at the top of each clay cap where deformation is minimal. CT scans offer a better view of sedimentary structures than the line-scan photographs. Since CT scans are three dimensional, they are not affected by artifacts resulting from core splitting and surface cleaning; instead, they highlight density contrasts that result from changes in sediment grain size and mineralogy (Zolitschka et al., 2015; Fortin et al., 2013). The lines marking the varve boundaries on the core images were saved in jpeg format. The coordinates of each varve boundary were measured using the freeware Fiji to calculate the thickness of each varve and saved in text format. In the present study, we use 1928 CE (22 BP, where "BP" is years prior to 1950 CE for both varve- and radiocarbon-based ages, and where ^{14}C ages are calibrated in calendar years), the first varve below the 1929 turbidite that corresponds to the failure of the first Eklutna Lake dam, as the topmost marker for our chronology. Details regarding the post-1929 sedimentology of Eklutna Lake can be found in Boes et al. (2018).

3.3. Tephra geochemistry

Tephra beds were located visually and by their high magnetic susceptibility values. Samples were removed from the split core face from approximately 2 mm below the magnetic susceptibility peak to 4 mm above the peak for a total thickness of approximately 6 mm. The samples were placed in 30% hydrogen peroxide to dissolve fine organic particles. Once rinsed, the samples were sieved using a 20 μm mesh and the fraction larger than 20 μm was density separated at 2.45 g/cm^3 to float the glass component for analysis.

Glass major-element geochemistry was analyzed on a JEOL 8900 electron microprobe at the University of Alberta, using wavelength dispersive spectrometry. A reduced current of 6 nA and a defocused beam of 10 μm diameter was used to minimize alkali loss during analyses; accelerating voltage was set at 15 keV. One subset of samples was analyzed using a new routine optimized for smaller shards and microlite-rich samples using a 5-μm-diameter beam and time-dependent intensity correction to compensate for Na loss through the Probe for EPMA software (Donovan et al., 2015). Two secondary standards, Lipari obsidian (ID3506) and Old Crow tephra, were analyzed concurrently with the unknown samples. Backscatter electron imaging was used to avoid analyzing glass shards with substantial microcrystalline inclusions and phenocrysts. Data from all individual analyses and standard data are available as supplementary data (Tables S3 and S4 and Figs. S1 and S2).

At least 30 glass shards were analyzed from each individual tephra sample. The major-element geochemistry of each sample was examined through bivariate plots to identify coherent geochemical populations and eliminate outliers. Outliers were defined as analyses with oxide values beyond the $\pm 2\sigma$ (3σ for wt% Na_2O) average of the primary geochemical population(s) or trends. Outliers are generally the result of accidental analysis of mineral microcrystals within the glass shards, or of detrital glass, with compositions that do not conform to the petrologically consistent geochemical trend of a sample. Detrital glass from does form a minor background component of the ambient sediment in Eklutna Lake and can complicate, in some cases, the interpretation of tephra data. However, the tephras presented here are well-defined units that show consistent geochemistry across all cores in which they were present, with little, if any, detrital glass contamination.

Table 1
Site characteristics and statistics of varve sequences.

Site number (Fig. 1)	2	3	4	20	21
Distance from inflow (m)	7200	4900	2300	1450	1200
Approx. water depth (m)	48	54.5	54.5	53	52
Length of the varved sequence (cm)	1138.0	1448.0	1606.5	764.9	754.5
Basal varve age (BP)	2309	2321	2182	919	854
Min. varve thickness (mm)	0.9	1.0	1.2	1.8	1.8
Mean varve thickness (mm)	5.0	6.3	7.4	8.5	9.0
Median varve thickness (mm)	4.1	4.7	5.9	7.0	6.8
Standard deviation varve thickness (mm)	3.9	6.9	7.0	7.1	15.5

3.4. Radiocarbon dating

Seven wood fragments were located using CT scans, handpicked and sent to the Chrono Lab of Queen's University in Belfast for accelerator mass spectrometry (AMS) radiocarbon dating. The samples were cleaned with an acid-base pretreatment and the $^{14}C/^{12}C$ and $^{13}C/^{12}C$ ratios were measured by AMS. The ^{14}C dates were calibrated using Calib 7.1 (Stuiver et al., 2018).

3.5. Chronological uncertainty

We used three independent approaches to assess the uncertainty of varve chronologies. The three approaches quantify different sources of the age uncertainty, namely: (1) subjectivity in identifying varves, (2) inter-site differences in varve counts, and (3) a combination of expert judgment about the likelihood of over- and under-counting and the proper identification of isochronous marker layers, with the constraint that the duration between marker layers must be consistent at all sites, which is a combination of (1) and (2).

Uncertainty ascribed to the subjectivity of observers has been routinely used to estimate the uncertainty in varve chronologies (Zolitschka et al., 2015; Ojala et al., 2012). Here we quantified the subjective error associated with recognizing varves on line-scan photographs and CT-scan images by comparing the varve counts made by two independent observers on four of the five cores. Both observers used the same counting method described above, and the difference in the number of varves was recorded for each core segment. This error was reported in two ways: (1) as a percentage of the total varve count per core section, which shows whether the difference is negative or positive, and (2) as semi-quantitative confidence intervals on our master chronologies (described below), where absolute values of count differences are applied to each side of the master chronology.

Following the comparison of varve counts, master varve chronologies were obtained by carefully reviewing the varve and marker-layer boundaries in an iterative process by two independent observers. The objective was to converge on the varve count for each core that minimized observer-dependent inconsistencies or biases. The chronological uncertainty of the master chronologies was then quantified using two other methods, described below.

Relying on multiple cores from the same lake together with well-defined marker beds, we used a cross-dating method (Lamoureux, 2001) to evaluate the uncertainty related to inter-site differences. We calculated the inter-site age variability of 34 well-defined marker layers that were confidently cross-correlated among two or more cores (Fig. 2). The age of each marker bed, according to the master chronology, was compared between cores and the age difference between each marker bed was expressed as a percentage for that bed. This method revealed the spatial and temporal distribution of varves across the lake, and hence enabled us to identify patterns of over- or under-counting (Ojala et al., 2012).

3.6. Bayesian model integration of uncertainty

To integrate information regarding age uncertainty, we developed a Bayesian model (the varve model code in R, including input and output files used in this study, is available at McKay, 2018). This model effectively integrates both a sedimentological understanding of the likelihood of the correct delineation of varves and marker layers with the constraint that all sites must have the same number of years (varves) between marker layers, even though that number is unknown. The model takes advantage of the replication and marker layers at the site to quantify the likelihood of over- and under-counting, as well as the ultimate uncertainty in varve years as a function of depth in each core. Consequently, the model is completely independent from ^{14}C or other age control, which serve as appropriate validation of the model and its uncertainty quantification.

There are three primary inputs to the model (Supplementary Table S2). The first is varve thickness (Table S2a). The second input is prior estimates of over- and under-counting probabilities for each varve in each core, that is, the likelihood that a counted varve should actually be two varves (under-counted) or that an identified varve should actually be part of an adjacent varve (over-counted) (Table S2b). The third input is the position of the marker layers found in two or more cores, and prior probability semi-quantitative estimates that each marker layer is properly identified and isochronous based on visual comparison of the layers (Table S2c).

We use here the difference in the number of varves counted between the two independent observers, expressed in percentage, as the prior value estimate for over- and under-counting. These percentages where applied symmetrically, with a higher difference between the counts translating into a higher chance that a varve count is either over- or under-counted.

Upon initialization, the algorithm heuristically updates the over- and under-counting priors based on observed differences in the counts between marker layers. The heuristic updates are only used to increase miscounting probabilities, and thus the originally assigned priors ultimately serve as minimum miscounting estimates. The model then proceeds to simulate 1000 iterations of the varve counts for each core. In each simulation, there are several steps. First, we sample from the marker layers proportionally to the prior estimates of each marker layer to select a subset of marker layers that are treated as correctly identified and isochronous for this simulation. Because this set of marker layers varies with each iteration, the impact of misidentification of the marker layers is included in this analysis. Then, for each segment (the interval of varves between a pair of marker layers), the probability of miscounting the number of varves between marker layers is used to simulate a "true" number of varves in that segment in each core. This simulation serves as the likelihood function in the simulation, and this step repeats until, by random, the number of simulated years between marker layers in all cores is identical. This step can be numerically challenging, especially as the number of cores increases. For example, consider a segment with 100 counted years: in five cores, each year could be over-counted, under-counted or correct for each core. The total number of permutations is therefore $5 * (3^{100}) = 2.5 \times 10^{48}$. Consequently, it is not possible to numerically search the full parameter space, and even finding a reasonable number of valid solutions requires some accommodations, including the heuristic adjustment to the prior described above. The second accommodation is, if the algorithm fails to find a solution for all cores, it iteratively removes one core, selected at random, from the simulation and attempts again. This continues until a solution is found, or until only two cores remain. Consequently, most iterations include gaps between marker layers for each core, but the coverage is robust across the 1000 ensemble members.

The 1000-member ensemble is then used to quantify the uncertainty in depth as a function of varve year, and can be transposed to estimated uncertainty in varve year as a function of depth in each core. By design, and largely due to the heuristic update of miscounting probabilities, the central tendency of the model output resembles the average counts across cores, as simulating the same number of varves is currently the only constraint on likelihood. Additional constraints on likelihood, such as independent age control and correlation of varve thicknesses across cores, are planned improvements to the model, but beyond the scope here.

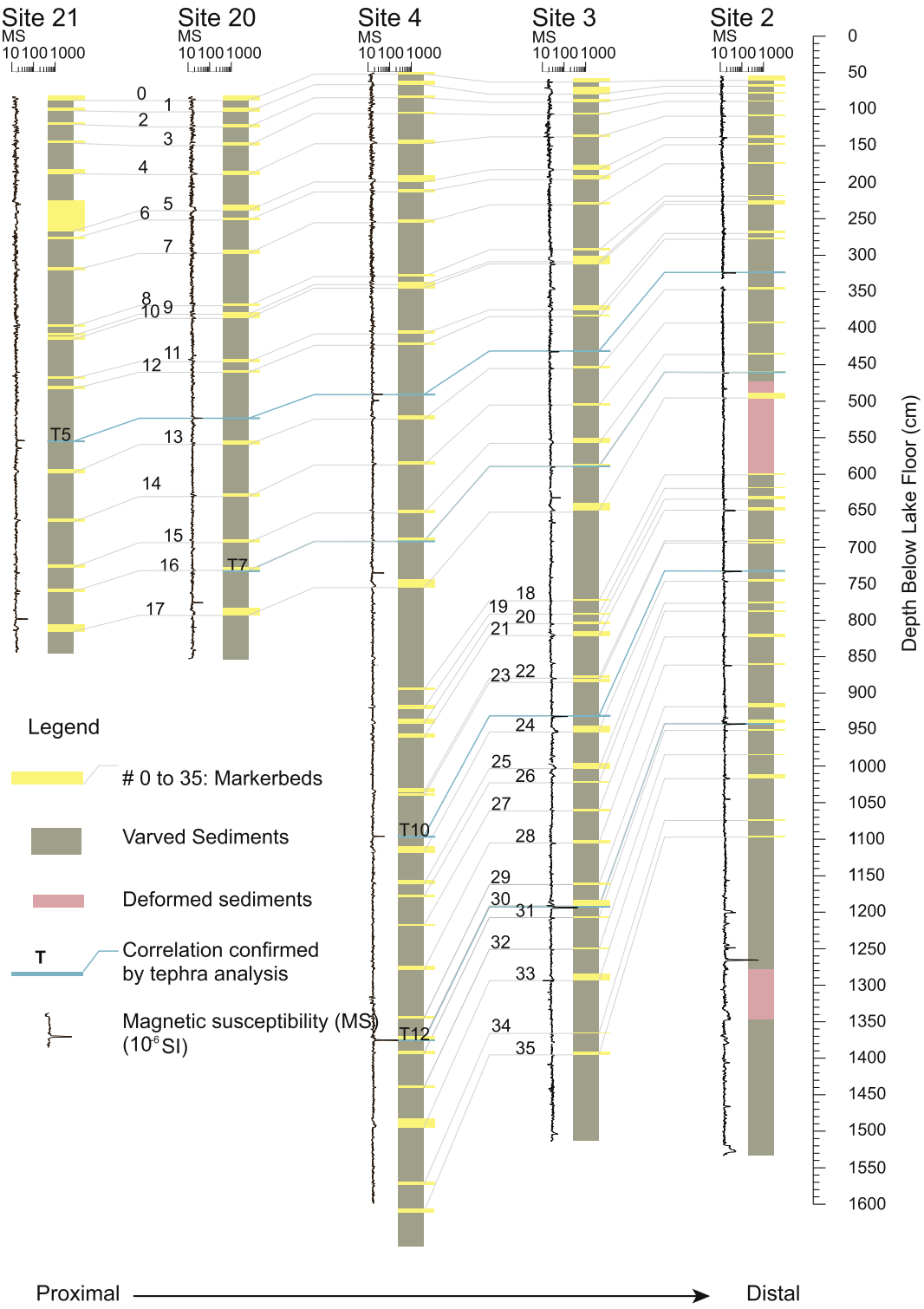

Fig. 2. Litho-stratigraphic logs, magnetic susceptibility (MS), tephra layers and marker-bed correlations for Eklutna Lake. Top of each log coincides with the 1929 AD marker layer, the topmost maker for our chronology. Core site locations shown in Fig. 1.

3.7. Age model verification and tephra tie lines

The varve-count uncertainty is a measure of the precision of the count but does not include undetected systematic errors that can influence the chronological accuracy as a result of over- or under-counting or missing layers (Zolitschka et al., 2015). To test the accuracy of the chronology, a comparison of varve counts with independent methods of dating is needed. In addition to verifying the robustness of the near-surface varve chronologies of Eklutna Lake surface cores using ^{137}Cs and historical events presented by Boes et al. (2018), seven radiocarbon dates on terrestrial macrofossils were compared to our longer varve chronologies.

Finally, we used four geochemically correlated tephra beds as well-defined tie lines to test whether their ages as represented in

different cores, overlap within the errors of our site-specific age models. Because the tephras were not included in the development of the age models, they serve as an independent test of the accuracy of the chronologies. In addition, we apply the age models to converge on the best age estimate for the four previously undated tephras.

4. Results and discussion

4.1. Sedimentary structures

Eklutna Lake sediments are composed of simple and complex varves, tephra beds visually recognizable by their contrasting color and grain size, crypto-tephra identified by spikes in magnetic susceptibility, and mass-wasting deposits (turbidites and slumps) resulting from seismic shaking such as the 1964 earthquake, from human-induced events such as the dam failure of 1929, and from high-energy flood events. The most common sedimentary unit found in Eklutna Lake sediments is the rhythmic layering typical of glacial varves, with a structure sometimes referred to as a "classic varve" (Zolitschka et al., 2015). These couplets consist of a layer of silt or very fine sand overlain by a clay-rich layer, or clay cap (Fig. 3A and B). In some instances, particularly in cores from the proximal basin near the inflow delta, varve structures can be complex (Fig. 3B), with two or more graded coarse-grained layers overlain by a clay cap. In other instances (Fig. 3C), the clay cap is interrupted by a thin (<1 mm) layer of coarser sediment.

Classic glacial varves are formed by deposition of coarse particles during the high-discharge season, followed by settling of fine particles, sometimes aided by flocculation, during fall and winter (de Geer, 1912; Hodder, 2009). Graded and complex varves appear to result from the succession of multiple high-energy fluvial pulses within one melt season, potentially from underflows, which are common in glacial-fed lakes (e.g., Schiefer and Gilbert, 2008; Desloges, 1994). Non-graded varves, mainly observed in the distal cores of Eklutna Lake, exhibit two units of homogenous grain size and are typically attributed to sedimentation from overflow plumes during the summer and the settling of clay during fall and winter (Ashley, 1975).

Thick, graded beds form a second type of sedimentary unit observed throughout the cores from all five sites (Fig. 3C and D). These are interpreted to be turbidites and are structurally similar to typical varves, with a fining-upward sequence that can be observed from both line-scan photographs and density contrast in the CT-scan images. However, they contain significantly coarser sediment at their base than beds identified as varves, with a more pronounced grading of the coarse-grained portion and an overall thickness of several times the average varve (Fig. 3C and D). Some turbidites show clear signs of erosion of underlying sediments, particularly in the proximal cores.

4.2. Varve counts and thicknesses

The five sediment cores display continuous couplets, interrupted by turbidites and tephras, that are interpreted as varves. Sites 21 and 20, located closest to the inflows (Fig. 1, Table 1), have varve chronologies that extend to 854 and 919 BP, respectively. Cores taken from the three other sites have chronologies that include over 2000 years of deposition. Varve thickness (VT) and standard variation of VT show a constant decline from proximal to distal positions relative to the inflow sites (summarized in Table 1, with thickness of each varve in Supplemental Table S2a). This pattern is consistent with sediments that are predominantly delivered as underflows or interflows, rather than from flocculation of sediment suspended in the water column (Hodder, 2009).

4.3. Varve counting uncertainty related to observer

The multiple-observer method is routinely used to obtain estimates of uncertainty in varve counts. It provides a strong

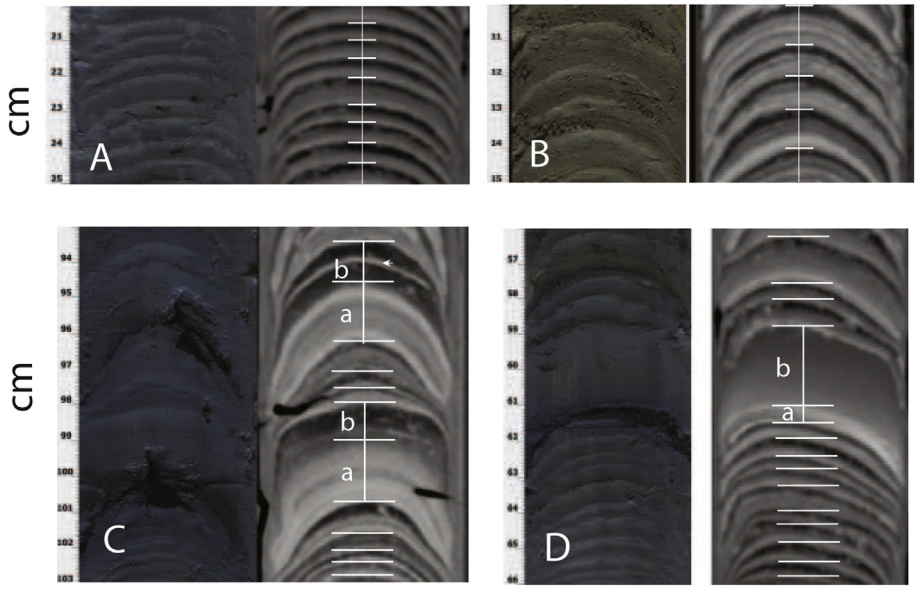

Fig. 3. Examples of typical varves (A, B) and turbidites (C, D) in cores from Eklutna Lake. For all panels, line-scan images are on the left and CT-scan topograms on the right. The coarse-grain layers appear dark on the photograph and pale on the topograms and inversely for the clay cap. The vertical white lines mark the transect along which thicknesses were measured and white horizontal lines mark varve boundaries as delimited by one observer. (A) Simple varves from distal site 2, section 02B-1P-2, 20–25 cm, each composed of two couplets. (B) Complex varves from proximal site 21 section 21B-1P-2, 10-15 cm, composed of more than one sub-annual layer of coarse sediments. (C) Sequence of two turbidites from site 2, section 02B-4P-2. Small white arrow in the upper turbidite marks a coarse layer that could be interpreted as a spring freshet event or as an interruption of the clay cap by a late summer pulse. (D) A simple turbidite from distal site 2, section 02B-1P-2, 56–66 cm, displaying a classic graded sequence. Lower-case letters "a" and "b" correspond to the initial coarse sediment pulse and subsequent fine-grain deposition, respectively.

indication of the subjective uncertainty associated with the visual delimitation of varves. It also gives an indirect measure of the clarity of varves, as greater differences between observers is to be expected in sections where varves are more difficult to discern (i.e. complex varves). In this study, this metric serves as a prior defining the likelihood that a core segment is over- or under-counted.

Two observers working independently counted the varves of sites 20, 4, 3, and 2 (Table 2). The cumulative uncertainty attributed to observer differences varies between less than 1% (site 20) to 7.5% (site 4). When calculated by individual core segments, the difference between counts ranges from 0.4% (site 3, section 03B-3P1) to 20.9% (site 4, section 04B-1G). The differences are both positive and negative, showing that both over- and under-counting occur and that neither observer had a systematic bias to count more or fewer varves. Because the percentage-wise error is calculated relative to the total number of varves by section, the short length of some core segments translates in some instances to high percentages that represent differences of only a few varves. This measure of uncertainty is likely associated with the visual clarity of the varves and points to sections in which varves are less clearly defined, a measure that is not captured by the other methods of uncertainty determination.

4.4. Cross-correlation of marker beds

Using the master varve chronology from each site, we compared the ages of 35 marker beds that were correlated across two or more cores (Fig. 2). Similar to the multiple-observer method, inter-site differences in varve counts can be calculated cumulatively for the entire sequence down to the lowest marker bed common to all cores, or for segments between each marker bed. The difference in cumulative varve counts represents a sum of both over-counting and under-counting of varves in addition to the potential absence of varves resulting from erosion. For consistency, the convention we use here is to compare distal cores to proximal cores.

The difference in the number of varves counted from above the lowest marker bed common to all cores (marker 17 = ca 800 BP) varies by a few percent, ranging from −5.3% between sites 2 and 20, to 2.6% between site 3 and 4 (Table 3). This overall cumulative uncertainty compares well with those reported from similar varve chronologies (Ojala et al., 2012). The differences between proximal and distal sites show some systematic tendencies. For example, site 2 has fewer varves above the lowest marker bed than all other sites (Table 3). This site is located in the distal basin 8 km from the inflow where varves are thinnest and likely difficult to recognize for years when inflows were low. Alternatively, multiple pulses within single years could have led to over-counting at the proximal sites. If so, we expect site 3 also to have fewer varves than the more proximal sites. Instead, site 3 has more varves, suggesting that some varves might be missing by erosion from the proximal sites, which have chronologies that extend back to around 850 BP. For sites with longer chronologies, a similar pattern emerges from the older part of the sequence, where site 2 exhibits fewer varves and site 3 exhibits more varves than site 4.

The age of each marker bed and the number of varves counted between each marker bed provides a more detailed account of chronological similarities and differences among sites (Table S2c). Overall the pattern is similar to that determined from the cumulative differences; site 2 is the most under-counted or has the most missing varves, followed by the three proximal sites. These results demonstrate that, if we had analyzed cores from only two sites, the range of difference could have been misleadingly smaller than what we obtained by comparing five cores.

Table 2
Number of varves counted per core segment by two independent observers (obs) with difference expressed in percent.

Section	Number of varves		% error
	Obs 1	Obs 2	
Site 2			
EK14-20C-1P-1	84	86	2.40
EK14-20C-1P-2	117	114	−2.60
EK14-20B-1P-1	58	59	1.70
EK14-20B-1P-2	71	75	5.60
EK14-20C-2P-1	153	148	−3.30
EK14-20C-2P-2	130	129	−0.80
EK14-20B-2P-1	116	122	5.20
EK14-20B-2P-2	213	201	−5.60
Total	**942**	**934**	**0.80**
Site 4			
EK14-04B-1G	82	105	21.90
EK14-04C-1P-1	81	84	3.57
EK14-04C-1P-2	117	127	7.87
EK14-04B-2P-1	50	51	1.96
EK14-04B-2P-2	83	89	6.74
EK14-04C-2P-1	176	182	3.30
EK14-04C-2P-2	183	190	3.68
EK14-04B-3P-1	48	52	7.69
EK14-04B-3P-2	109	118	7.63
EK14-04C-3P-1	205	218	5.96
EK14-04C-3P-2	180	212	15.09
EK14-04B-4P-1	67	69	2.90
EK14-04B-4P-2	202	210	3.81
EK14-04C-4P-1	174	193	9.84
EK14-04C-4P-2	203	220	7.73
EK14-04B-5P-1	41	43	4.65
EK14-04B-5P-2	230	249	7.63
Total	**2231**	**2412**	**7.50**
Site 3			
EK14-03A-1H	137	140	2.14
EK14-03C-1P-1	30	33	9.09
EK14-03C-1P-2	142	150	5.33
EK14-03B-1P-1	31	32	3.13
EK14-03B-1P-2	61	60	−1.67
EK14-03C-2P-1	169	176	3.98
EK14-03C-2P-2	176	189	6.88
EK14-03B-2P-1	112	110	−1.82
EK14-03B-2P-2	164	160	−2.50
EK14-03C-3P-1	180	186	3.23
EK14-03C-3P-2	81	82	1.22
EK14-03B-3P-1	234	235	0.43
EK14-03B-3P-2	146	139	−5.04
EK14-03C-4P-1	244	251	2.79
EK14-03C-4P-2	272	279	2.51
EK14-03B-4P-1	65	61	−6.56
EK14-03B-4P-2	184	189	2.65
Total	**1499**	1529	**−2.00**
Site 20			
EK14-02A-1G	204	178	−14.61
EK14-02B-1P-1	55	52	−5.77
EK14-02B-1P-2	210	211	0.47
EK14-02A-2P-1	59	56	−5.36
EK14-02A-2P-2	243	232	−4.74
EK14-02B-2P-1	230	212	−8.49
EK14-02B-2P-2	55	52	−5.77
EK14-02A-3P-1	290	271	−7.01
EK14-02A-3P-2	318	290	−9.66
EK14-02B-3P-1	225	208	−8.17
EK14-02B-3P-2	85	75	−13.33
EK14-02A-4P-1	313	298	−5.03
EK14-02A-4P-2	114	118	3.39
Total	**2401**	**2253**	**−6.57**

4.5. Bayesian varve model outputs

The model outputs are presented as age-depth curves with their 95% high-density region (HDR) along with the master varve chronology and the multiple-observer uncertainty ensemble for each site (Fig. 4). The outputs from the model represent a varve age that

Table 3
Cumulative error based on the age difference at the lowest marker bed of each core.

	Cumulative error (% difference)			
	Site 3	Site 4	Site 20	Site 21
Site 2	−3.4	−1	−5.3	1.3
Site 3		2.6	−1.7	2.3
Site 4			1.7	−0.5
Site 20				1.1

is consistent with the miscounting and marker-layer priors, as well as the varve counts in the other cores from Eklutna Lake. The modeled age-depth curves suggest that the initial varve count from site 3 was systematically over-counted (i.e., the initial varve ages were older than the median modeled age) and that sites 20 and 21 were over-counted in their lower sections. Conversely, varves at the most distal site 2 appear to be systematically under-counted. Some of this is by design in the model; since the model does not incorporate any information external to the varve counting, it will not, for example, suggest that all sites are over-counted. The chronology at site 4 is, however, in broad agreement with the original counts, displaying slight evidence for over- or under-counting at different depths in the cores.

These model results are in general agreement with our interpretation from the master varve counts. For example, the model indicates that site 2 is under-counted, in accordance with our analysis based on marker-bed ages of the master chronology. Before circa 850 BP, the model shows a near perfect match with the varve count of site 4, while site 2 is appears to have been under-counted and site 3 over-counted. However, as shown by the relatively large difference between the counts of two observers, the varve counts from sites 4 and 2 are more prone to error than site 3. Also, site 4, due to its proximal location is subject to erosive events and site 2 has intervals of less well defined varves, both of which could lead to under-counting relative to site 3.

Age uncertainties derived from the Bayesian model output can be summarized using probability distributions of the modeled ages of the 34 marker beds (Fig. 5). As exemplified by maker bed 1, the

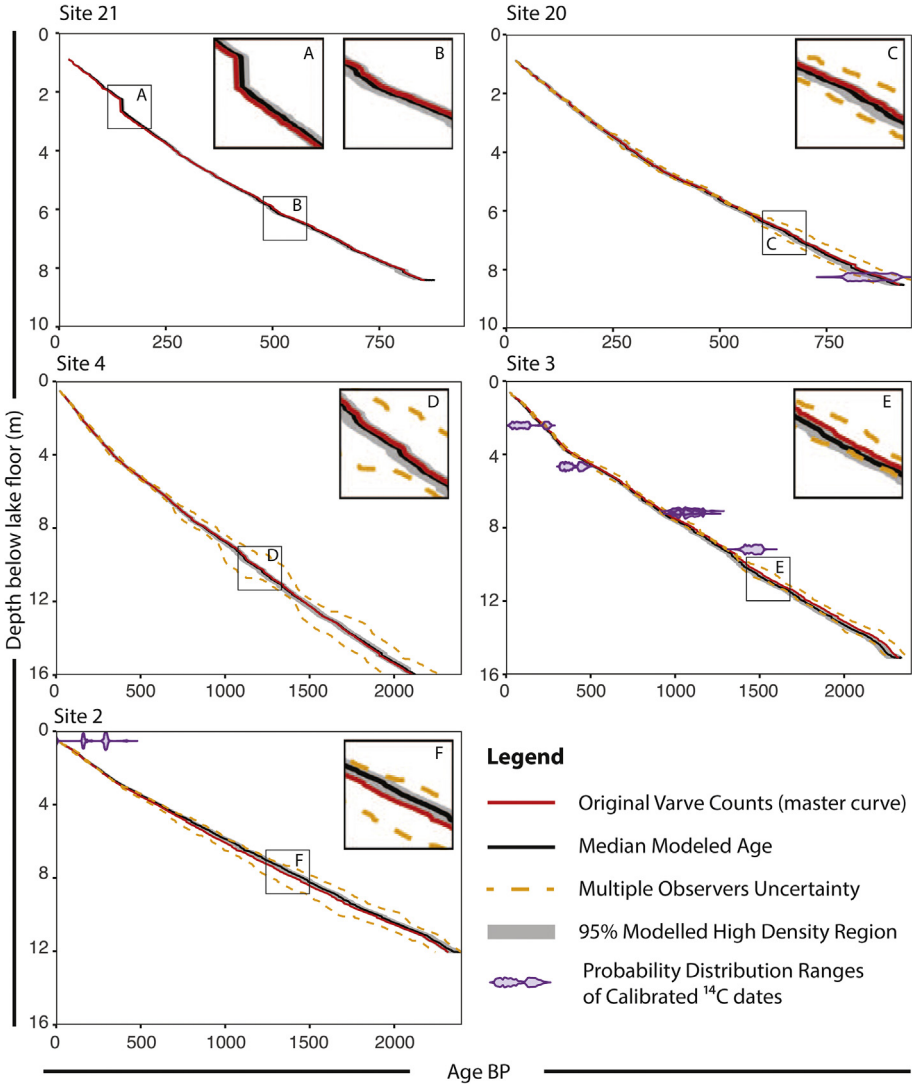

Fig. 4. Age models for the five core sites with modeled uncertainty and radiocarbon ages. The sites are arranged from proximal (site 21) to distal (site 2). Inserts A to F provide a more detailed view of some of the key difference between age models. Red line is the age-depth profile according to the master varve chronology. Black line is the median modeled age with the 95% high-density region in grey. Orange dashed line represents the qualitative varve-count uncertainty. The probability distribution ranges of calibrated ^{14}C ages are shown as purple shapes. Note that temporal and depth scales for sites 21 and 22 are different from the other sites. Age BP is years before 1950 CE. (For interpretation of the references to color in this figure legend, the reader is referred to the Web version of this article.)

modeled ages closely follow the varve ages of the markers, which is expected because the varve age of these layers was the primary input to the model. In most cases the model assigns an age that corresponds roughly to the average age of the marker bed as determined by varve counts. In some instances, such as for marker beds 27 and 35, the distribution of modeled ensemble ages is skewed, reflecting the presence of an outlier among the varve ages.

4.6. Age-model validation using ^{14}C

A total of eight radiocarbon dates on terrestrial macrofossils were acquired from three of the cores, with six from site 3 (Table 4, Fig. 4). One of the ages from near the surface of site 3 yielded an untenable median age of 5818 cal BP and was rejected, likely indicating remobilization of wood stored on the landscape and transferred to the lake thousands of years later. The age with wide-ranging age distribution near the surface of site 2 likely reflects similar remobilization of an old wood fragment. Assuming that the material dated is the same age as the sediment that encloses it, the radiocarbon ages from site 3 point toward over-counting before 500 BP, a period marked by thicker and more complex varves, and under-counting before 1000 BP, while the single ^{14}C age from site 20 is in good agreement with both the master varve chronology and the modeled age. At site 3, the two-sigma range of the calibrated radiocarbon dates are older than the master varve chronology and the modeled varve ages.

4.7. Age-model validation using tephra tie lines

In addition to tephra analysis presented here, Boes et al. (2018) correlated two tephra layers located above the 1929 CE marker bed with historical eruptions. For our study, the major-element composition of glass shards was analyzed on four tephras that could be easily traced among three or more core sites using

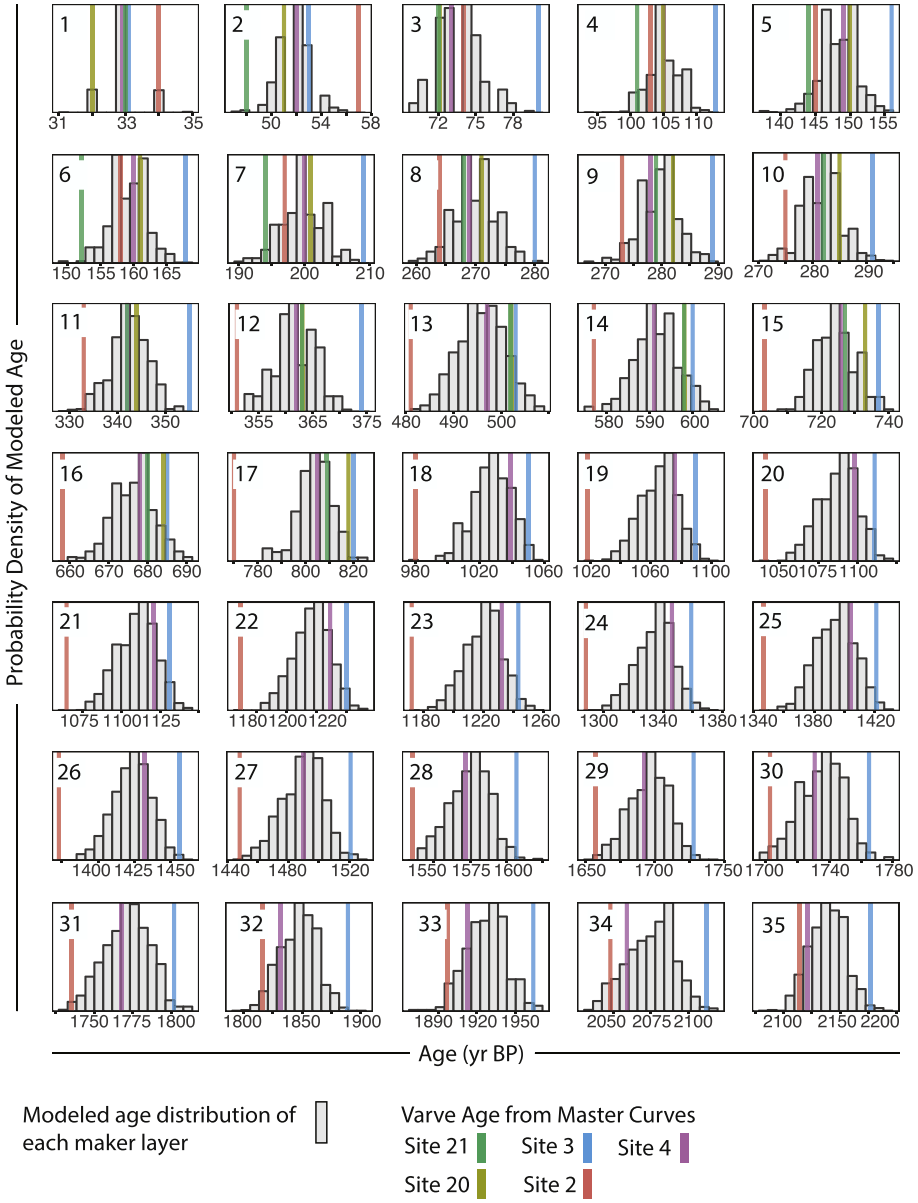

Fig. 5. Histograms of modeled age distribution for each marker bed, showing the age of the bed as determined in each core. Depths of marker beds are shown in Fig. 2. Median age for each marker bed is listed in Table S2c.

Table 4
Radiocarbon ages.

Site	Core segment	Composite depth (cm blf)	Material	$\delta^{13}C$ (‰)	^{14}C age (yr BP)	±	Median calibrated age (yr BP)	One-half of 2-sigma range
2	EK14-02A-1G	52.8	wood	−25.4	236	30	284	211
3	EK14-03C-1P-2	242.3	wood	−23.0	98	29	111	124
3	EK14-03C- 2P-2	466.7	flower or seed		346	20	387	83
3	EK14-03B- 2P-2	723.0	seed		1157	31	1074	97
3	EK14-03C-3P-1	709.0	wood	−33.7	1154	44	1072	107
3	EK14-03C- 3P-2	918.1	unidentified		1559	28	1467	70
20	EK14-20B-2P-2	825.2	wood	−28.8	932	26	853	64

Note: ^{14}C ages calibrated using CALIB7.1 (Stuiver et al., 2018).

magnetic susceptibility data. The overlapping geochemical compositions (Fig. 6) confirm the stratigraphic correlations. These tephra beds offer independent tests of our age models, which in turn can be used to assign an age to the tephras. The ages of all tephra layers show close agreement among the cores (Table 5), which confirms that the chronologies are in close agreement with each other. None of these tephras have been definitively correlated with any previously described units due to a lack of reference material, thus they do not offer any additional independent age information to the model. However, as discussed below, their ages all correspond with known eruptions from their assumed source volcanoes.

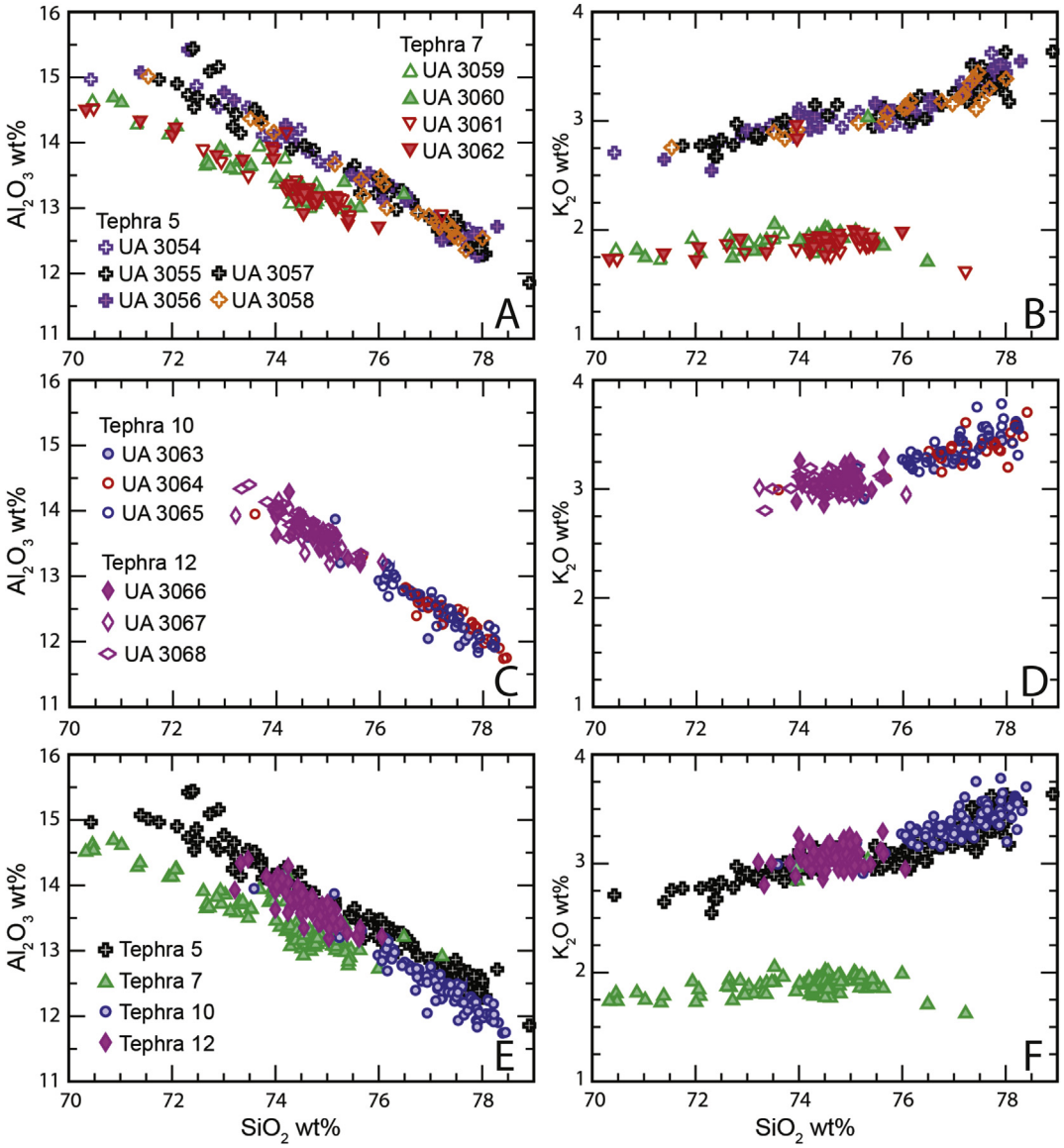

Fig. 6. Bivariate plots of major-element geochemistry of individual glass shards expressed in oxides as weight percent (wt%). (A, B) Tephras 5 and 7 sampled from five and four cores, respectively. (C, D) Tephras 10 and 12 sampled from three cores each. (E, F) Comparison of all four tephra beds based on data from all sampled cores. The full suite of major-element geochemical data is available in Table S4.

Table 5
Summary of tephra ages.

Tephra	Site	Varve age (yr BP)	Bayesian model median age (yr BP)	±1 SD	Inter-quartile range (yr)
Tephra 5	21	455	452	5	7
	20	456	455	5	7
	4	451	454	5	7
	3	462	454	5	7
	2	430	454	5	7
Tephra 7	20	732	727	7	8
	4	726	728	6	8
	3	737	729	6	8
	2	700	730	7	10
Tephra 10	4	1317	1310	13	16
	3	1329	1311	13	17
	2	1256	1315	13	17
Tephra 12	4	1738	1754	15	20
	3	1769	1743	15	21
	2	1700	1750	15	20

4.8. Tephra geochemistry and potential sources

The tephras currently have informal names that follow the simple scheme started by Boes et al. (2018) who correlated magnetic susceptibility peaks across surface cores and named them from youngest to oldest, Tephra 1, 2, 3 … etc. Boes et al. (2018) presented geochemical data for Tephra 1, which was identified as Crater Peak 1992, and Tephra 2, identified as Redoubt 1990. The tephras discussed here are Tephras 5, 7, 10 and 12 (Table 6). Tephras 5, 10 and 12 have geochemical compositions that are very similar to and/or on the geochemical trend defined by reference material from Redoubt eruptions in 1990 and 2009 (Fig. S1). This is not surprising considering the location of the lake and its relative proximity to Redoubt Volcano. Tephra 7 has a distinctly lower K_2O content and higher Cl that is often a defining geochemical characteristic of Augustine Volcano, another very active volcano in the Cook Inlet region (e.g., Siebert et al., 1995; Blockley et al., 2015; Fig. S1). Potential alternative sources with somewhat similar geochemistry are Hayes volcano, which is closer to Eklutna Lake, and Kaguyak, farther south on the Alaska Peninsula. However, mid-Holocene tephra from Hayes volcano tends to have $K_2O > 2.0$ wt% and lower FeO_t (Fig. S1), post-caldera activity at Kaguyak appears to be largely andesitic and limited to lava flows, and there is no evidence at either Hayes or Kaguyak for activity overlapping in time with Tephra 7 (e.g., Fierstein and Hildreth, 2008; Wallace et al., 2014). On the other hand, Tephras 5, 7, 10 and 12 were all deposited at times roughly coincident with eruptive events previously described from Redoubt and Augustine (e.g., Begét and Nye, 1994; Begét et al., 1994; Waitt and Begét, 2009; Schiff et al., 2010). In particular, Waitt and Begét's (2009) summary of Augustine describes several eruption events, namely Augustine Tephra B and M, whose potential age ranges overlaps with the date of Tephra 7, with Tephra B averages and standard deviations showing some similarities with Tephra 7 (Fig. S1; Siebert et al., 1995).

A lack of available reference data has made it difficult to firmly establish correlations with previously described regional tephra. However, Payne and Blackford (2008) present a cryptotephrostratigraphy from a peat core near Skilak Lake on Kenai Peninsula, about 140 km southwest of Eklutna Lake, that contains two shard-abundance peaks around the same time as the deposition of Tephra 5 (~454 BP) and 7 (~729 BP). Tephra ST-24 (ca. 1480 CE) comprises two geochemical populations, but one of the populations roughly plots with Tephra 5 (Fig. S2). The other shard-abundance peak, ST-36 (ca. 1230 CE), also contains some geochemical scatter but plots relatively well with Tephra 7 (Fig. S2). It is difficult to ascertain without standard data from Payne and Blackford (2008) if the slight offsets are real differences or analytical; however, these data do suggest that these two tephras could be widely distributed markers in southern Alaska.

5. Conclusions

1. We present varve chronologies from five core locations totaling 57 m of sediments from Eklutna Lake. Our basin-wide, cross-correlated chronology extends to 2250 BP and represents the longest continuous published varve chronology from Alaska.
2. Increasing the number of cores taken from the same lake increases the apparent age uncertainty (i.e., differences in varve counts among core sites) but reveals a clearer picture of the source of the chronological uncertainty. Over- and under-counting and erosion can account for inter-site difference in varve chronologies.
3. The Bayesian model presented here for the first time integrates classic methods of estimating the chronological uncertainty of varves to produce most likely age models. Our model generates an age for any core depth and offers a new way to quantify age uncertainty in inter-correlated varved sequences. Future refinements of the model could use varve thickness to constrain inter-site correlations.
4. We present new data for four tephra layers, three of which were likely from Redoubt Volcano (Tephras 5, 10 and 12), and one most likely from Augustine Volcano (Tephra 7). The detailed geochemistry provided, combined with their high-resolution ages, make them important marker horizons for future studies in Alaska.

Table 6
Summary of tephra glass major-element geochemistry for correlated marker layers, normalized to 100%. Full suite of shard-by-shard major-element geochemistry is available in Table S3.

Name		SiO_2	TiO_2	Al_2O_3	FeO_t	MnO	MgO	CaO	Na_2O	K_2O	Cl	H_2O_d	n
Tephra 5	Mean	75.67	0.26	13.44	1.37	0.07	0.28	1.54	4.10	3.13	0.14	2.40	126
	StDev	1.97	0.08	0.88	0.40	0.02	0.13	0.49	0.30	0.23	0.04	1.87	
Tephra 7	Mean	74.04	0.44	13.49	2.33	0.06	0.58	2.53	4.29	1.92	0.31	0.54	101
	StDev	1.33	0.08	0.55	0.35	0.02	0.14	0.42	0.26	0.26	0.06	1.25	
Tephra 10	Mean	77.11	0.26	12.49	1.19	0.05	0.21	1.18	3.97	3.37	0.17	2.87	88
	StDev	0.90	0.05	0.45	0.18	0.02	0.07	0.26	0.15	0.18	0.03	1.26	
Tephra 12	Mean	74.66	0.30	13.70	1.68	0.08	0.32	1.65	4.38	3.06	0.17	2.27	72
	StDev	0.54	0.04	0.28	0.18	0.03	0.05	0.11	0.12	0.10	0.03	1.02	

Note: n = number of analyses; FeO_t = all Fe as FeO; H_2O_d = water by difference (100 − original total).

Acknowledgements

DF, NPM and DSK were funded by NSF awards 1418000 and 1602106. NP and MDB were funded by the Research Foundation Flanders (FWO-Vlaanderen grant G042812N). We are grateful to Doug Steen and Christopher Benson for help with the multiple-observer varve counts, Adrian Bender, Kristi Wallace and an anonymous reviewer for input on an earlier version of the manuscript, Chugach State Park for its interest in this work, and R. Achten and E. Van de Moortel for use of the CT scanner at Ghent University Hospital. Any use of trade, firm, or product names is for descriptive purposes only and does not imply endorsment by the U.S. Government.

Appendix A. Supplementary data

Supplementary data to this article can be found online at https://doi.org/10.1016/j.quascirev.2018.10.018.

References

Ashley, G.M., 1975. Rhythmic sedimentation in glacial Lake Hitchcock, Massachusetts-Connecticut. In: Jopling, A.V., McDonald, B.C. (Eds.), Glaciofluvial and Glaciolacustrine Sedimentation, vol. 23. Society of Economic Paleontologists and Mineralogists Special Publication, pp. 304–320.

Begét, J.E., Nye, C.J., 1994. Postglacial eruption history of Redoubt Volcano, Alaska. J. Volcanol. Geoth. Res. 62, 31–54. https://doi.org/10.1016/0377-0273(94)90027-2.

Begét, J.E., Stihler, S.D., Stone, D.B., 1994. A 500-year-long record of tephra falls from Redoubt Volcano and other volcanoes in upper Cook Inlet, Alaska. J. Volcanol. Geoth. Res. 62, 55–67.

Blockley, S.P., Edwards, K.J., Schofield, J.E., Pyne-O'Donnell, S.D., Jensen, B.J., Matthews, I.P., Cook, G.T., Wallace, K.L., Froese, D., 2015. First evidence of cryptotephra in palaeoenvironmental records associated with Norse occupation sites in Greenland. Quat. Geochronol. 27, 145–157.

Boes, E., Van Daele, M., Moernaut, J., Schmidt, S., Jensen, B.J.L., Praet, N., Kaufman, D., Haeussler, P., Loso, M.G., De Batist, M., 2018. Varve formation during the past three centuries in three large proglacial lakes in south-central Alaska. Geol. Soc. Am. Bull. 130, 757–774. https://doi.org/10.1130/B31792.1.

Brabets, T.P., 1993. Glacier Runoff and Sediment Transport and Deposition: Eklutna Lake Basin, Alaska. U.S Geological Survey, p. 52. Water-Resources Investigations Report 92-4132.

de Geer, G., 1912. A geochronology of the last 12,000 years. In: 11th International Geological Congress (1910), Stockholm, Sweden, vol. 1, pp. 241–253.

Desloges, J.R., 1994. Varve deposition and the sediment yield record at three small lakes of the southern Canadian Cordillera. Arct. Alp. Res. 26, 130–140.

Donovan, J., Kremser, D., Fournelle, J.H., Goemann, K., 2015. Probe for EPMA: Acquisition, Automation and Analysis. Probe Software Inc.. www.probesoftware.com

Fierstein, J., Hildreth, W., 2008. Kaguyak dome field and its Holocene caldera, Alaska Peninsula. J. Volcanol. Geoth. Res. 177, 340–366.

Fortin, D., Kaufman, D.S., Arnold, M., Schiefer, E., Hawley, N., 2015. Late-summer peak in sediment accumulation in two lakes with contrasting watersheds, Alaska. Geografiska Annaler Series A 97, 709–719.

Fortin, D., Francus, P., Gebhardt, A.C., Hahn, A., Kliem, P., Lisé-Pronovost, A., Royschowdhury, R., Labrie, J., St Onge, G., The PASADO Science Team, 2013. Destructive and non-destructive density determination: method comparison and evaluation from the Laguna Potrok Aike sedimentary record. Quat. Sci. Rev. 71, 147–153.

Hodder, K.R., 2009. Flocculation: a key process in the sediment flux of a large, glacier fed lake. Earth Surf. Process. Landforms 34, 1151–1163.

Hollinger, K., 2002. The Early Electrification of Anchorage. Center for Environmental Management of Military Lands, Colorado State University, p. 66. CEMML TPS 02-8.

Karlstrom, T.N.V., 1964. Quaternary Geology of the Kenai Lowland and Glacial History of the Cook Inlet Region, Alaska. U.S. Geological Survey Professional Paper 443, 69 pp.

Lamoureux, S.F., 2001. Varve chronology techniques. In: Last, W.M., Smol, J.P. (Eds.), Developments in Paleoenvironmental Research (DPER) Volume 1: Basin Analysis, Coring, and Chronological Techniques. Kluwer, Dordrecht, pp. 247–260.

Larquier, A.M., 2010. Differing Contributions of Neavily and Moderately Glaciated Basins to Water Resources of the Eklutna Basin, Alaska. M.Sc. Thesis,. Alaska Pacific University, Anchorage, Alaska.

Mankhemthong, N., Doser, D.I., Pavlis, T.L., 2013. Interpretation of gravity and magnetic data and development of two-dimensional cross-sectional models for the Border Ranges fault system, south-central Alaska. Geosphere 9, 242–259.

Marshall, M., Schlolaut, G., Nakagawa, T., Lamb, H., Brauer, A., Staff, R., Bronk-Ramsey, C., Tarasov, P., Gotanda, K., Haraguchi, T., Yokoyama, Y., Yonenobu, H., Tada, R., 2012. A novel approach to varve counting using μXRF and X-radiography in combination with thin-section microscopy, applied to the late glacial chronology from Lake Suigetsu, Japan. Quat. Geochronol. 13, 70–80.

McKay, N.P., 2018. Varve Model Code, v0.1.0. https://doi.org/10.5281/zenodo.1272157.

Ojala, A.E.K., Francus, P., Zolitschka, B., Besonen, M., Lamoureux, S.F., 2012. Characteristics of sedimentary varve chronologies - a review. Quat. Sci. Rev. 43, 45–60.

Payne, R., Blackford, J.J., 2008. Distal volcanic impacts on peatlands: palaeoecological evidences from Alaska. Quat. Sci. Rev. 27 (21–22), 2012–2030.

Praet, N., Moernaut, J., Van Daele, M., Boes, E., Haeussler, P.J., Strupler, M., Schmidt, S., Loso, M.G., De Batist, M., 2017. Paleoseismic potential of sublacustrine landslide records in a high-seismicity setting (south-central Alaska). Mar. Geol. 384, 103–119.

Riihimaki, C.A., MacGregor, K.R., Anderson, R.S., Anderson, S.P., Loso, M.G., 2005. Sediment evacuation and glacial erosion rates at a small alpine glacier. J. Geophys. Res. 110, F03003.

Sass, L.C., Loso, M.G., Geck, J., Thoms, E.E., 2017. Geometry, mass balance and thinning at Eklutna Glacier, Alaska: a balance feedback with implications for water resources. J. Glaciol. 63–289, 343–354.

Schiefer, E., Gilbert, R., 2008. Proglacial sediment trapping in recently formed Silt Lake, upper Lillooet Valley, coast Mountains, British Columbia. Earth Surf. Process. Landforms 33, 1542–1556.

Schiff, C.J., Kaufman, D.S., Wallace, K.L., Ketterer, M.E., 2010. An improved proximal tephrochronology for Redoubt Volcano, Alaska. J. Volcanol. Geoth. Res. 193, 203–214.

Siebert, L., Beget, J.E., Glicken, H., 1995. The 1883 and late-prehistoric eruptions of Augustine Volcano, Alaska. J. Volcanol. Geoth. Res. 66, 367–395.

Staff, R.A., Nakagawa, T., Schlolaut, G., Marshall, M.H., Brauer, A., Lamb, H.F., Bronk Ramsey, C., Bryant, C.L., Brock, F., Kitagawa, H., van der Plicht, J., Payne, R.L., Smith, V.C., Mark, D.F., MacLeod, A., Blockley, S.P.E., Schwenninger, J.-L., Tarasov, P.E., Haraguchi, T., Gotanda, K., Yonenobu, H., Yokoyama, Y., Suigetsu 2006 Project Members, 2013. The multiple chronological techniques applied to the Lake Suigetsu SG06 sediment core, central Japan. Boreas 42, 259–266.

Stuiver, M., Reimer, P.J., Reimer, R.W., 2018. CALIB 7.1. WWW program. http://calib.org. (Accessed 12 May 2018).

Tian, J., Brown, T.A., Hul, F.S., 2005. Comparison of varve and ^{14}C chronologies from Steel Lake Minnesota, USA. Holocene 15, 510–517.

Waitt, R.B., Begét, J.E., 2009. Volcanic Processes and Geology of Augustine Volcano. Alaska. U.S. Geological Survey Professional Paper 1762, 78 pp.

Wallace, K., Coombs, M.L., Hayden, L.A., Waythomas, C.F., 2014. Significance of a Near-source Tephra-stratigraphic Sequence to the Eruptive History of Hayes Volcano, South-Central Alaska. U.S. Geological Survey Scientific Investigations Report, pp. 2014–5133, 32 pp.

Wilson, F.H., Hults, C.P., 2013. Geology of the Prince William Sound and Kenai Peninsula Region, Alaska. U.S. Geological Survey, Open-File Report 2008-1002.

Zolitschka, B., Francus, P., Ojala, A.E.K., Schimmelmann, A., 2015. Varves in lake sediments - A review. Quat. Sci. Rev. 117, 1–41.